

Lattice Boltzmann simulation of viscous fluid systems with elastic boundaries

Haiping Fang, Zhifang Lin, and Zuowei Wang

T D Lee Physics Laboratory and Department of Physics, Fudan University, Shanghai 200433, China

(Received 11 April 1997; revised manuscript received 6 October 1997)

A lattice Boltzmann model able to simulate viscous fluid systems with elastic and movable boundaries is proposed. By introducing the virtual distribution function at the boundary, the Galilean invariance is recovered for the full system. As examples of application, the flow in elastic vessels is simulated with the pressure-radius relationship similar to that of the pulmonary blood vessels. The numerical results for steady flow are in good agreement with the analytical prediction, while the simulation results for pulsative flow agree with the experimental observation of the aortic flows qualitatively. The approach has potential application in the study of the complex fluid systems such as the suspension system as well as the arterial blood flow.
[S1063-651X(98)50701-5]

PACS number(s): 47.60.+i, 47.10.+g, 87.45.-k

The study of viscous fluid systems with elastic or movable boundaries has attracted much attention over forty years (see, e.g., [1,2]) due to their great relevance to the arterial blood flow as well as the suspension system in the field of complex fluids. As the need to account for the effect of changeable geometries adds considerably to the difficulty of the analysis, numerical simulation plays a major role in this field.

Conventional methods for simulating viscous fluid flow include, macroscopically, numerical integration of the Navier-Stokes equations, and, microscopically, molecular-dynamics simulation. The former is, however, particularly difficult to implement in complex and changeable geometries, while the latter is extremely computationally intensive. An alternative approach, the lattice Boltzmann method (LBM) [3,4], has recently proved competitive in studying the domain of fluid flow for various physical systems [5]. Derived from the lattice gas automata (LGA) [6], the LBM inherited from the LGA most of its major advantages over the conventional computational method. It is easy to implement and parallel in nature due to the fact that all the information transfers in local time and space. And compared with the LGA, the LBM may suppress the statistical noise and satisfy the requirement of the Galilean invariance.

Although numerical accuracy of the LBM is of second order inside the fluid, an inappropriate implementation of boundary conditions will substantially degrade the LBM. Several boundary treatments have thus been proposed for achieving second-order accuracy [7-9], but most of them are restricted to the systems with fixed geometries. In addition, all current approaches neglect the requirement of the Galilean invariance at the solid-fluid boundary, which is of critical importance for the fluid systems with elastic or movable boundaries.

In this Rapid Communication we propose a lattice Boltzmann model that is capable of simulating viscous fluid systems with elastic and movable boundaries. This is achieved by introducing virtual distribution functions (VDF's) at the boundary. With this model, numerical accuracy up to second order is attained, and the recovery of the Galilean invariance for *the full systems including boundary* is shown by analytical analysis and verified by numerical calculation. As examples of application for the model, the viscous flow in elas-

tic vessels is simulated with the pressure-radius relationship similar to that of the pulmonary blood vessels [10]. The numerical results for steady flow are in excellent agreement with the analytical prediction, and the simulation results for pulsative flow agree with that of the aortic flows observed experimentally [11]. These results, together with the simplicity and the ease of implementation of the model, suggest that our approach may be a promising tool in studying the blood flow in arteries, especially in the diseased ones that suffer from atherosclerosis, stenosis, or aneurysm. It is also expected that the model may find applications in numerical simulation of the suspension in the complex fluid systems [12].

Let us first recall some basic ideas of the LBM in the domain of fluid flow. We choose to work on a square lattice in two dimensions. Let $f_i(\mathbf{x}, t)$ be a non-negative real number describing the distribution function (DF) of the fluid density at site \mathbf{x} at time t moving in direction \mathbf{e}_i . Here $\mathbf{e}_0 = (0, 0)$, $\mathbf{e}_i = (\cos \pi(i-1)/2, \sin \pi(i-1)/2)$, $i = 1, 2, 3, 4$, and $\mathbf{e}_i = (\cos \pi(i-4-\frac{1}{2})/2, \sin \pi(i-4-\frac{1}{2})/2)$, for $i = 5, 6, 7, 8$ are the nine possible velocity vectors. The DF's evolve according to a Boltzmann equation that is discrete in both space and time:

$$f_i(\mathbf{x} + \mathbf{e}_i, t + 1) - f_i(\mathbf{x}, t) = \Omega_i(\mathbf{x}, t). \quad (1)$$

The most convenient choice for $\Omega_i(\mathbf{x}, t)$ is a single time relaxation form [3]

$$\Omega_i(\mathbf{x}, t) = -\frac{1}{\tau}(f_i - f_i^{eq}). \quad (2)$$

The density ρ and macroscopic velocity \mathbf{u} are defined by

$$\rho = \sum_i f_i, \quad \rho \mathbf{u} = \sum_i f_i \mathbf{e}_i, \quad (3)$$

and the equilibrium DF's f_i^{eq} are usually supposed to be dependent only on the local flow velocity \mathbf{u} . A suitable choice of which makes the macroscopic equations recover the Navier-Stokes equations by a Chapman-Enskog procedure [3].

We next describe the DF's at the boundary. For clarity of the following description, let us define some concepts. In

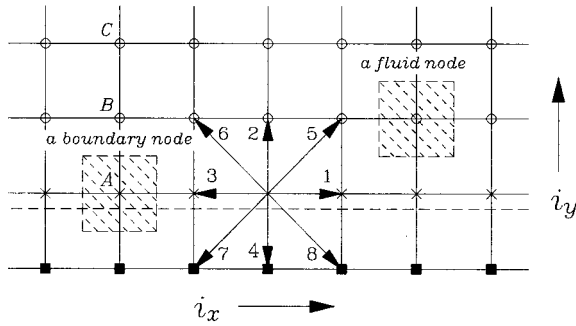


FIG. 1. Schematic plot of part of the lattice system we considered. The dashed line is a bottom boundary, below which is an impermeable wall. The solid box represents the nodes inside the impermeable wall, the open circles are FN's, and the crosses denote BN's. The shaded square centered at A is the square associated with the node A.

Fig. 1 we show an example. The dashed line is a bottom boundary, under which is an impermeable (physical) wall, which will be called wall nodes (WN's) hereafter. Similarly, the open circles in the domain of fluid are the fluid nodes (FN's) and the crosses denote the boundary nodes (BN's).

Associated with each lattice node is a square of unit sides centered at the node, as shown in Fig. 1 by the shaded part. Then, a node is a BN if any physical boundary crosses its square (see, e.g., node A in Fig. 1).

It is clear that only part of the square of the BN is filled with fluid, so the real fluid density at the BN is significantly less than those at its neighbored FN's. However, in any lattice Boltzmann scheme, the sums of DF's at neighbored nodes should be about the same. To this end, we introduce VDF's $g_i(\mathbf{x}, t)$ at the BN, so that the sum of which is approximately the same as those of the DF's at its neighbored FN's.

We now describe the VDF $g_i(\mathbf{x}, t)$ at the BN for flat wall, say node A shown in Fig. 1. In each streaming step,

$$g_i(\mathbf{x}, t) = f_i(\mathbf{x} - \mathbf{e}_i), \quad \text{if the node at } \mathbf{x} - \mathbf{e}_i \text{ is an FN,}$$

$$g_i(\mathbf{x}, t) = g_i(\mathbf{x} - \mathbf{e}_i), \quad \text{if the node at } \mathbf{x} - \mathbf{e}_i \text{ is a BN,}$$

$g_i(\mathbf{x}, t)$ is determined from nonslip condition as in [7]

$$\text{if the node at } \mathbf{x} - \mathbf{e}_i \text{ is a WN,} \quad (4)$$

where i may be 0, 1, ..., 8, whereas the velocity at the BN needed to determine g_i as in [7] is obtained by quadratic extrapolation or interpolation. Then the collision step of the single time relaxation type is applied to $g_i(\mathbf{x}, t)$ at any BN. However, after collision, $g_i(\mathbf{x}, t)$ is scaled such that $\sum_{i=0}^8 g_i(\mathbf{x}, t)$ equals ρ^v , where ρ^v is given by extrapolation [8],

$$\rho^v = 2\rho^1 - \rho^2, \quad (5)$$

with ρ^1 and ρ^2 being the densities at the FN's on the first layer and second layer (nodes B and C in Fig. 1). This extra scale step prevents the sum of VDF's at the BN from varying dependent on the component of velocity normal to the

boundary, and keeps it approximate to the fluid density at neighbored FN's, as required by the LBM. Moreover, the scale step helps guarantee the Galilean invariance for the simulation results (see below).

As yet we have not described the real DF $f_i(\mathbf{x}, t)$ at the BN. Since there should be no VDF at any FN, we assume, at the BN for the flat wall and after collision,

$$f_i(\mathbf{x}, t) = g_i(\mathbf{x}, t), \quad \text{if the node at } \mathbf{x} + \mathbf{e}_i \text{ is an FN,}$$

$$f_i(\mathbf{x}, t) = 0, \quad \text{if the node at } \mathbf{x} + \mathbf{e}_i \text{ is a BN or WN,} \quad (6)$$

$$f_0(\mathbf{x}, t) = \rho(\mathbf{x}, t) - \sum_{j=1}^8 f_j(\mathbf{x}, t),$$

where i may be 1, ..., 8, and ρ is the real fluid density at the BN (see below). Equation (6) leads to the fact that only fluid particles propagate between the BN and its neighbored FN's, while only virtual particles propagate between neighbored BN's for the flat wall. When a WN just becomes a BN due to the motion of wall, the real fluid density at this node $\rho = 0$. In the subsequent streaming steps, the density at the BN may increase or decrease, depending on the velocities at the BN and the neighbored FN's as well as the density at the neighbored FN's.

At the BN for the nonflat wall, the VDF's are still given by Eq. (4) except those for $g_i(\mathbf{x}, t)$ with the nodes $\mathbf{x} - \mathbf{e}_i$ being WN's, which are obtained by generalizing the method in [7], mainly based on the bounce-back rule for the nonequilibrium part of the DF normal (or approximately normal) to the boundary. The velocity needed to determine the VDF's at the BN is evaluated by an average of extrapolated (interpolated) values of two or more directions, and so is ρ^v in the scale step. For the real DF's at the BN, on the other hand, the second equation of Eq. (6) should also be modified, in order to guarantee the Galilean invariance. Some fluid particles, in addition to virtual particles, are assumed to stream among neighbored BN's. Due to the limitation in length, the full algorithm for the VDF's and the real DF's at the BN for the nonflat wall, together with its applications in systems with (fixed and changeable) complex geometries, are presented elsewhere [13].

Now we show that the technique guarantees that the LBM results recover the Galilean invariance. Consider a channel with a flat wall moving with a fixed velocity $\mathbf{u} = (u_x, u_y) = (u, v)$, where u and v are the components of the velocity parallel and perpendicular to the channel, respectively. Without loss of generality, we assume $v > 0$. After the system becomes stable, all nodes (both FN's and BN's) share the same and time-independent DF's (VDF's at BN's). Then it follows from Eqs. (4) and (6) that the increment of the fluid density at any BN of the upper boundary in each time step is $g_2 + g_5 + g_6 - g_4 - g_7 - g_8$, which equals $\rho^v v$ [see Eq. (3)], where $\rho^v = \rho_0$ [see Eq. (5)], with ρ_0 being the density at any FN. Let t_0 be the time that a WN at \mathbf{x} becomes a BN and t_1 the time when the BN turns to an FN, i.e.,

$$\text{a WN} \xrightarrow{\text{at } t_0} \text{a BN} \xrightarrow{\text{at } t_1} \text{an FN.} \quad (7)$$

Then one has the fluid density $\rho(\mathbf{x}, t_0) = \rho_0$, and $\sum_{t=t_0}^{t_1} v \Delta t = 1$. Here $\Delta t = 1$ is the time step. As a result, the density at the node at t_1 reads

$$\rho(\mathbf{x}, t_1) = \sum_{t=t_0}^{t_1} \rho^v v \Delta t = \rho^v \sum_{t=t_0}^{t_1} v \Delta t = \rho_0. \quad (8)$$

This new FN, therefore, has the same density as other FN's, yielding no perturbation when any BN becomes an FN. Similar results can be obtained for the process

$$\text{an FN} \rightarrow \text{a BN} \rightarrow \text{a WN} \quad (9)$$

as well. Thus all the FN's and BN's will always share the same velocity \mathbf{u} , and the fluid in the channel from our simulation is static if one observes it in a moving frame of reference with velocity \mathbf{u} . We verify this by numerical simulation accurate up to the machine accuracy.

With the present scheme, the LBM results recover the Galilean invariance to the second order for many other systems. It can be proved that the increment of the fluid density at any BN in each time step is $\rho^v v$ to second order [13]. It follows from Eq. (8) that the perturbation is small enough during the process (7) provided that the variance of ρ^v is of second order. Things are similar for the process (9). In the following we take the plane Poiseuille flow as an example. For this system with a fixed velocity component v_0 perpendicular to the pipe, the velocity $\mathbf{u} = (u_x, u_y) = (u, v)$ is obtained from the Navier-Stokes equations analytically,

$$u = u_0 [1 - (y - v_0 t)^2 / a^2], \quad v = v_0, \quad (10)$$

for $|y - v_0 t| \leq a$, where $u_0 = -a^2 (\partial p / \partial x) / 2\rho v$, a is the width of the pipe, p the pressure at x , ρ the density, and v the viscosity. We have carried out simulations with a variety of τ , v_0 , and u_0 . The range of τ is from 0.6 to 10.0; v_0 varies from 0.0001 to 0.01; and u_0 from 0.0001 to 0.015. In the period of Eq. (7), our simulation results show that the maximal value of the error err_y is less than 10^{-4} , where

$$\text{err}_y = \frac{|u_y^{th}(\mathbf{x}) - u_y(\mathbf{x}, t)|}{|u_y^{th}(\mathbf{x})| + |u_y(\mathbf{x}, t)|}, \quad (11)$$

with $u_y^{th}(\mathbf{x})$ being the analytical velocity at node \mathbf{x} , and $u_y(\mathbf{x}, t)$ the velocity at node \mathbf{x} at time t from numerical simulation. The $u_x(\mathbf{x}, t)$ from our simulation is accurate up to second order as that shown in Refs. [7,8].

As examples of application for the present model, we perform simulations of a long and thin plane elastic pipe with length L . The pressure $p(x)$ to width $a(x)$ relationship is assumed to be linear:

$$p(x) - p_0 = \alpha(a(x) - a_0), \quad (12)$$

where a_0 is the width when the pressure inside is fixed to be p_0 ; α is a compliance constant. In the three-dimensional case with a being the tube radius, Eq. (12) is a good representation of the pulmonary blood vessels [10]. Denoting the pressure at inlet and outlet by $p(0)$ and $p(L)$, respectively, we assume $p(0) > p(L)$. Since the pipe is long and thin, that is, $L \gg a$, and the pipe is smooth under deformation, the ve-

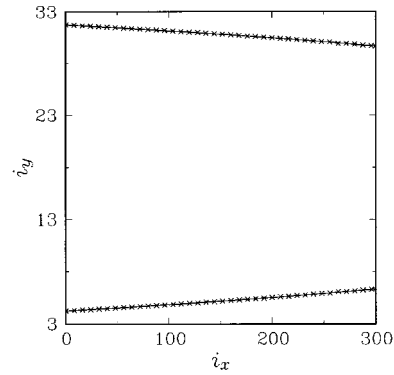


FIG. 2. The analytical prediction (—) and numerical simulation (\times) of the boundaries of a long and thin elastic pipe along the channel.

locity can be approximated by that of the plane Poiseuille flow [10]. After some algebra, we obtain, for steady flow, a theoretical formula for the width $a(x)$, which is a function of position x for $0 < x < L$ because of the elastic deformation:

$$a^4(x) - a^4(0) = Bx, \quad B = -3vQ/\alpha, \quad (13)$$

where Q is the volume-flow rate, which is a constant throughout of the pipe in a stationary, nonpermeable pipe. From this equation the pressure $p(x)$ is given by

$$\left(a_0 + \frac{p(x) - p_0}{\alpha}\right)^4 - \left(a_0 + \frac{p(0) - p_0}{\alpha}\right)^4 = Bx. \quad (14)$$

For our LBM simulation, the pipe is 300 units in length so that each (upper or bottom) boundary is composed of 300 small parts with unit length. The mass for each part is 500. Denote the momentum change at a BN by δp_c in each step. Then the force acting on the corresponding part is δp_c , which in turn gives the velocity of the part and its displacement from the equilibrium location. The simulation results for steady flow are shown in Fig. 2 for the upper and bottom boundaries, and in Fig. 3 for the pressure. It is seen that the results are, respectively, very consistent with the analytical predictions (13) and (14). In our numerical simulation, $a_0 = 13.5$, $\alpha = 0.01$, and $\tau = 2$.

Finally, we present our simulation results on the pulsative flow in elastic pipes. The pipe is L units in length and 30 units in width initially with both sides closed. At discrete time $t = T, 2T, \dots, nT, \dots, 1/810$ of the total fluid particles in the pipe are injected into the pipe from the left side and ejected out of the pipe from the right side simultaneously. The fluid will then flow from left to right. Figure 4 displays the typical volumetric flow wave forms (VFW's) through the cross section at the middle of the pipe for $T = 725$. It is striking to find that the VFW's for $L = 600$ and $L = 350$ are quite similar to the experimental results for the aortic flow and the left anterior descending coronary flow (see Fig. 5 in [11]). There is backflow and an inflexion (or dip) before the vfw reaches its peak each time, resulting from the elastic behavior of the pipe. Considering that the simulation is performed in two dimensions while the experiment is in three dimensions, the agreement between our simulation results and the experimental ones [11] is rather satisfactory. These

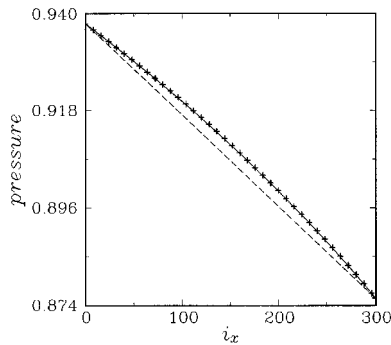


FIG. 3. The analytical prediction (—) and numerical simulation (+) of the pressure in the same elastic pipe of Fig. 2. The dashed line is a linear connection between the beginning and ending points, which should be the result for a rigid pipe.

results suggest that the present model may provide an alternative approach to simulating the blood flow in an artery.

To summarize, we have described a lattice Boltzmann model that is able to simulate viscous fluid system with movable boundaries, the main new feature of which is the introduction of VDF's at BN's. This enables us to obtain an overall lattice Boltzmann model that satisfies the requirement of the Galilean invariance macroscopically. As examples of application, both the steady flows and the pulsative flows in elastic pipes are simulated. The former is found to be in excellent agreement with the theoretical prediction, while the latter shows pulsative behavior comparing favorably with that of the aortic flows observed experimentally.

It should be noted that the conventional methods for simulating blood flow in an artery include numerical integration of the Navier-Stokes equations [14], which is extremely computationally intensive and particularly difficult to implement in complex geometries, especially for the diseased arteries that suffer from atherosclerosis, stenosis, or aneurysm. With the present model, such systems can be easily simu-

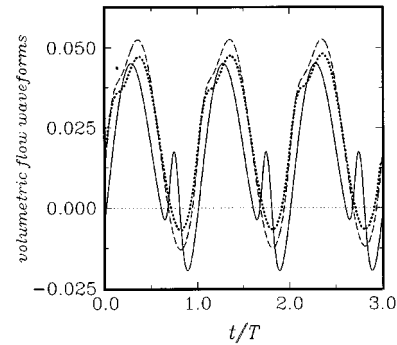


FIG. 4. The VFW's with respect to time t for a time period of $3T$ in an elastic pipe for $L=350$ (solid line) and $L=600$ (dashed line). Also shown in the figure (dotted line) is a plot of vfw's with respect to time in an elastic vessel with the masses for some parts of the wall decreased by 60% (see text for details).

lated by simply changing the masses and the elastic constants of the corresponding parts of the vessel wall along with its geometry. In Fig. 4, we show, as an example, the typical VFW for a simple model of diseased arterial vessel. The model is obtained from the system with $L=600$ by simply decreasing by 60% the masses for the parts of both (upper and lower) walls that located at a distance of 200 to 210 units from the left end. Compared with the result for the system with uniform mass distribution (dashed line in Fig. 4), the change in pulsative behavior of the VFW for the diseased model (dotted line in Fig. 4) is clearly seen. More numerical results on this subject as well as the bifurcation behavior of the arteries had already been obtained [13]. In addition, the model may also provide an alternative and competitive approach in simulating some complex fluid systems such as moving objects in a fluid (see, e.g., [15]) and suspension system [12]. Work along this line is also in progress.

We are indebted to Professor Ruibao Tao for his stimulating discussion. This work was partly supported by NSFC Grant No. 19704003.

-
- [1] G. W. Morgan and J. P. Kiely, *J. Acoust. Soc. Am.* **26**, 323 (1954); J. R. Womersley, *Philos. Mag.* **46**, 199 (1955).
- [2] S. A. Berger, *Contemp. Math.* **141**, 479 (1993).
- [3] S. Chen *et al.*, *Phys. Rev. Lett.* **67**, 3776 (1991); Y. H. Qian, D. d'Humières, and P. Lallemand, *Europhys. Lett.* **17**, 479 (1992).
- [4] R. Benzi, S. Succi, and M. Vergassola, *Phys. Rep.* **222**, 145 (1992).
- [5] A. K. Gunstensen *et al.*, *Phys. Rev. A* **43**, 4320 (1991); D. Grunau, S. Chen, and K. Eggert, *Phys. Fluids A* **5**, 2557 (1993); S. P. Dawson, S. Chen, and G. Doolen, *J. Chem. Phys.* **98**, 1514 (1993); D. H. Rothman, and S. Zaleski, *Rev. Mod. Phys.* **66**, 1417 (1994); D. Martinez, S. Chen, and W. H. Matthaeus, *Phys. Plasmas* **1**, 1851 (1994); G. R. McNamara, A. L. Garcia, and B. J. Alder, *J. Stat. Phys.* **81**, 395 (1995); W. R. Osborn *et al.*, *Phys. Rev. Lett.* **75**, 4031 (1995); N. S. Martys and H. Chen, *Phys. Rev. E* **53**, 743 (1996).
- [6] U. Frisch, B. Hasslacher, and Y. Pomeau, *Phys. Rev. Lett.* **56**, 1505 (1986); S. Wolfram, *J. Stat. Phys.* **45**, 471 (1985).
- [7] Q. Zou and X. He, *Phys. Fluids* **9**, 1591 (1997).
- [8] S. Y. Chen, D. Matinez, and R. W. Mei, *Phys. Fluids* **8**, 2527 (1996).
- [9] D. P. Ziegler, *J. Stat. Phys.* **71**, 1171 (1993); P. A. Skordos, *Phys. Rev. E* **48**, 4823 (1993); D. R. Noble *et al.*, *Phys. Fluids* **7**, 203 (1995); O. Behrend, *Phys. Rev. E* **52**, 1164 (1995); R. S. Maier, D. W. Grunau, and R. S. Bernard, *Phys. Fluids* **8**, 1788 (1996); I. Ginzbourg and D. d'Humières, *J. Stat. Phys.* **84**, 927 (1996); Z. Lin, H. Fang, and R. Tao, *Phys. Rev. E* **54**, 6323 (1996).
- [10] Y. C. Fung, *Biodynamics Circulation* (Springer-Verlag, Berlin, 1984).
- [11] J. Peacock *et al.*, *J. Biomech.* **28**, 17 (1995), and references therein.
- [12] M. A. van der Hoef, D. Frenkel, and A. J. C. Ladd, *Phys. Rev. Lett.* **67**, 3459 (1991).
- [13] H.-P. Fang and Z.-F. Lin (to be published).
- [14] H. Huang, V. J. Modi, and B. R. Seymour, *Contemp. Math.* **141**, 337 (1993).
- [15] G. H. Ristow, *Phys. Rev. E* **55**, 2808 (1997).